AN APPROACH TO THE PARAMETRIC DESIGN OF ION THRUSTERS†

Paul J. Wilbur††
Colorado State University
Fort Collins, Colorado 80523, U.S.A.

and

John R. Beattie* and Jay Hyman, Jr.**
Hughes Research Laboratories
Malibu, California 90265, U.S.A.

ABSTRACT

A methodology that can be used to determine which of several physical constraints can limit ion thruster power and thrust, under various design and operating conditions, is presented. The methodology is exercised to demonstrate typical limitations imposed by grid system span-to-gap ratio, intragrid electric field, discharge chamber power per unit beam area, screen grid lifetime and accelerator grid lifetime constraints. Limitations on power and thrust for a thruster defined by typical discharge chamber and grid system parameters when it is operated at maximum thrust-to-power are discussed. It is pointed out that other operational objectives such as optimization of payload fraction or mission duration can be substituted readily for the thrust-to-power objective and that the methodology can be used as a tool for mission analysis.

INTRODUCTION

Ion thrusters are very attractive propulsion devices not only because of their high efficiency and high specific impulse capabilities but also because they afford designers and potential users a great deal of design and operational flexibility. It is generally recognized, however, that operational flexibility (e.g. throttleability) carries with it a price of a greater system complexity that may not be justifiable for many missions and it should be noted that design flexibility also has its unattractive aspects. It can for example conjure up impressions, particularly in the minds of those who do not work directly with ion thrusters, that they are too complex. In order to overcome this concern, the work described herein has been undertaken and a framework within which ion thruster performance and design information can be presented in a simple, easily understood way has been sought. It is hoped that this methodology can be used to facilitate communication, teaching, and an identification of the most productive areas for research and development in support of a variety of propulsion system objectives.

The development of this methodology might be pursued in terms of empirical relationships following the techniques used by Byers and Rawlin[1] and by Byers[2] but the desire to use it for teaching purposes coupled with the fact that basic models describing ion thrusters have become available since their work was published, has prompted us instead to base the development on basic physical models. Where parameters are required in this development to accommodate non-ideal behavior, every attempt has been made to use parameters that are physically meaningful, commonly used and theoretically based. The objective of this paper is to present a methodology that can be used to establish a link between thruster design, operational and mission parameters in order to determine which of many possible performance-limiting phenomena will dominate in a particular situation. A second objective is ~~to~~ to establish a technique that can be used to present information on this subject in a manner that is both easy to visualize and understand.

THEORY

The cannonical design variables associated with an ion thruster are the specific impulse at which it operates (I_{sp}), its beam area (A_B) and its beam power (P_B). Generally, one would want to prescribe the specific impulse and beam area of a device and then determine the beam power at which it could be operated under a given set of design, operational and mission constraints, so in this development specific impulse and beam area will be treated as independent variables and beam power will be treated as the dependent variable.

Examples of physical constraints which have been found to limit the beam power at which a thruster can operate include:

Grid system span-to-gap ratio. This constraint is determined by ones ability to hold grids close together in an environment of thermally induced distortion and in some situations significant electrostatic attraction. It is influenced greatly by mechanical design and fabrication considerations and while a value of 600 might be considered a reasonable limit for conventional circular grids,[3] the use of intragrid supports or non-circular (e.g. annular or rectangular grids) could facilitate substantial increases above 600.

Intragrid electric field. Excessively high electric fields between the screen and accelerator grids of a thruster result in electrical breakdown and an inability to extract an ion beam. This limit is influenced by such factors as the surface finish and uniformity of the intragrid spacing and typical values in operating thrusters have generally been about 2 kV/mm[4] although much higher values have been reported.

Discharge power per unit beam area. This is actually a heat transfer limit that is imposed because components such as magnets, anodes or grids can overheat if the heat removal rate is inadequate. This constraint could be formulated in terms of specific heat transfer limitations for particular components but for the illustrative purposes of this paper, it will be assumed that the allowable discharge power scales directly with beam area and that a limit in the range 15 to 30 kW/m² is reasonable.

†Work supported in part by NASA Grant NGR-06-002-112.
††Professor, Dept. of Mechanical Engg., Member AIAA.
*Head, Plasma Sources Section, Ion Physics Dept., Member AIAA.
**Manager, Ion Physics Dept., Member AIAA.

Screen grid lifetime. The lifetime of the screen grid as well as other components exposed to the discharge plasma is limited by the process of ion-induced sputter erosion. Typically grids and other components have been designed to have lifetimes in the range of 10^4 to 2×10^4 hours. These lifetimes are influenced by the materials and ions involved and by the discharge voltage.

Accelerator grid lifetime. The accelerator grid is exposed to small currents of high energy, charge-exchange ions that limit its lifetime through sputter erosion. This grid is typically designed to have a lifetime in the same 10^4 to 2×10^4 hr range that the screen grid has.

The above list of constraints on ion thruster design is not exhaustive, but they represent constraints that have been encountered and they can be used for purposes of illustration.

A trade-off exists between the propellant and power requirements for an ion thruster and for this reason a preferred operating point or **operational objective** exists. The one selected influences the severity of each of the design constraints identified above. Once an objective that requires operation, for example, at the point where the thruster will produce maximum thrust per unit input power or maximum payload fraction on a prescribed mission has been identified, one can define the extent of the power limits cited in the preceding paragraphs. For the purposes of this study it will be assumed that the thruster is to be operated at the point of maximum thrust-to-power, but it should be recognized that this additional input, which could be much more complex, might come for example from an algorithm that optimizes a mission objective.

Mathematical Development

The beam power (P_B) produced by an ion thruster is expressed most simply as the product of beam current (J_B) and beam (or net accelerating) voltage (V_B).

$$P_B = J_B V_B \tag{1}$$

The beam current in this equation is related to the peak current density being extracted through the grids (j_{max}) and the beam area (A_B) through the beam flatness parameter ($\mathbb{F}$) which is defined as the ratio of average-to-peak ion beam current density.

$$\mathbb{F} = J_B/(j_{max} A_B) \tag{2}$$

It is noted that the flatness parameter can be calculated for a given discharge chamber using the finite element technique developed by Arakawa[5].

The maximum current density capability of a grid set is determined by space-charge limitations which may be described approximately using the one-dimensionally based Child-Langmuir law[6].

$$j_{max} = \frac{4 \epsilon_o}{9} \left[\frac{2e}{m_i}\right]^{1/2} \frac{V_T^{3/2}}{\ell_e^2} \phi_s \psi_e \tag{3}$$

The permittivity of free space (ϵ_o), the electron charge (e) and the ion mass (m_i) appearing in this equation are known constants and the total accelerating voltage (V_T) and the screen grid transparency to ions (ϕ_s) are at the control of the designer and/or operator. The ion current density enhancement factor (ψ_e) is a factor that will be set equal to unity for the purposes of this paper, but it could take on values greater than unity to account for the increased current density capabilities of grids when ions approach the screen grid plasma sheath at non-zero velocities[6] or high energy electrons are injected into the sheath[7] to mitigate the space-charge limitations that develop there. The final factor in Eq. 3, the effective ion acceleration length (ℓ_e), is the one that is limited by span-to-gap and electric field considerations and the imposition of these constraints will be considered in detail next. It will be assumed that the value of ℓ_e is the same for each aperture set over the entire grid surface for this development.

The total accelerating voltage that appears in Eq. 3 can eliminated in favor of the beam voltage by introducing the net-to-total accelerating voltage ratio (R)

$$R = V_B/V_T \ . \tag{4}$$

The beam voltage can be related to the specific impulse (I_{sp}) by recognizing that the specific impulse is defined as the thrust (F) per unit weight flowrate of propellant ($\dot{m} g_{eo}$)

$$I_{sp} = F/\dot{m} g_{eo} \ , \tag{5}$$

that the thrust is given by the momentum equation

$$F = [\dot{m} \eta_u] \left[U F_t \alpha\right] \ , \tag{6}$$

and that the ion exhaust velocity (U) is related to the beam voltage through the conservation of energy expression

$$V_B e = m_i U^2/2 \ . \tag{7}$$

In Eq. 6 the product of propellant mass flowrate ($\dot{m}$) and propellant utilization efficiency (η_u), which is the first bracketed term, represents the flowrate of thrust producing (high velocity) propellant and the second bracketed term represents the effective jet velocity of the beam ions along the thruster axis. This second term includes two thrust correction factors, one (F_t) that reflects the fact that many ions will emerge from the grid system on divergent trajectories[8] and a second (α) that accounts for the fact that Eq. 7 describes the velocity of singly charged ions only when in fact some multiply charged ions will generally be produced and extracted.[8]

Combining Eqs. 5, 6 and 7 the desired expression for beam voltage in terms of specific impulse is obtained

$$V_B = \frac{m_i}{2e} \left[\frac{I_{sp} g_{eo}}{\eta_u F_t \alpha}\right]^2 \tag{8}$$

and this may be combined with Eqs. 1 through 4 to obtain

$$P_B = \frac{\epsilon_o \mathbb{F} A_B \phi_s \psi_e}{9 \ell_e^2 R^{3/2}} \left[\frac{m_i}{e}\right]^2 \left[\frac{I_{sp} g_{eo}}{\eta_u F_t \alpha}\right]^5 \ . \tag{9}$$

Equation 9 defines the maximum power constraint associated with the ion extraction process for an ion thruster as a function of its beam area and the specific impulse at which it is to operate. Two physical constraints, one associated with the allowable span-to-gap ratio and the other with the maximum allowable electric field between the grids, actually evolve from this equation through the effective ion acceleration length (ℓ_e). The fact that propellant utilization appears in the equation also serves as a reminder that an operational objective must be defined before unique limiting values of beam power can be computed as a function of specific impulse and beam area for these two physical constraints.

Span-to-Gap Ratio Constraint

The allowable span-to-gap ratio (N) associated with traditional grid sets is the grid diameter-to-spacing ratio. In order to accommodate non-circular beam cross sections, however, this ratio will be

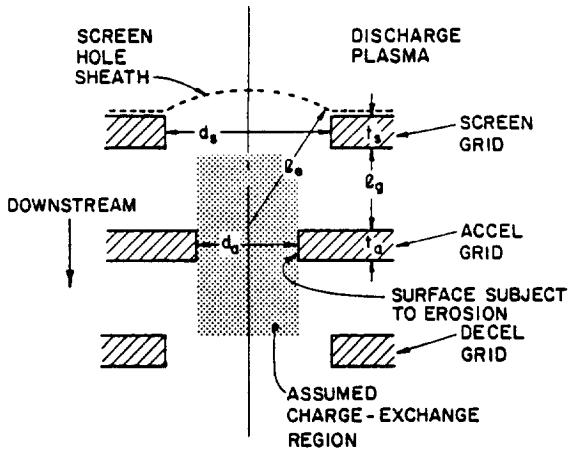

Fig. 1. Aperture System Geometry

defined here using an equivalent beam diameter and the grid separation will be given by the expression

$$\ell_g = \frac{\sqrt{4 A_B/\pi}}{N} \quad . \tag{10}$$

The preferred ion acceleration length for use in Eq. 9 (which is based on one-dimensional theory) would be the one that would yield the beam current density actually extracted from screen/accel grid aperture pairs in what is really a two-dimensional process. One value of ℓ_e that should come close to doing this is illustrated in Fig. 1 and examination of the geometry of this figure suggests ℓ_e is related to the grid separation distance given by Eq. 10 through the expression

$$\ell_e = \sqrt{(t_s + \ell_g)^2 + d_s^2/4} \quad . \tag{11}$$

It should be noted here that Eq. 11 differs from the traditional equation for ℓ_e used to compute perveances[9] in that it accounts for the screen grid thickness (t_s). If the screen grid thickness is left out of this expression, the implication is that the screen hole sheath positions itself close to the downstream edge of the screen grid. Aston[10] has shown, however, that this sheath tends to position itself near the upstream edge of the hole under normal operating conditions and Eq. 11 is therefore considered correct.

Equations 9, 10 and 11 can be combined to define the maximum beam power at which a thruster with a beam area A_B and a span-to-gap ratio N can be operated at prescribed specific impulses provided an operational objective, a screen grid thickness (t_s) and a screen hole diameter (d_s) are specified. For this illustrative study these latter two parameters have been defined by specifying a grid separation-to-screen hole diameter ratio (ℓ_g/d_s) and screen grid thickness of unity and 0.0005 m respectively.

Electric Field Constraint

In order to prevent electrical breakdown between grids it is presumed that a limiting electric field E cannot be exceeded. Assuming a uniform grid spacing, this may be expressed mathematically using the expression

$$\ell_g = \frac{V_T}{E} = \frac{V_B}{R\,E} \quad . \tag{12}$$

Combining this with Eqs. 9 and 11, an operational objective, a screen grid thickness and a screen hole diameter, the beam power/beam area/specific impulse surface limited by electrical breakdown considerations is defined.

Discharge Chamber Thermal Constraint

If the power required to operate a discharge chamber becomes too great, such failures as those associated with magnet, screen grid or anode overheating could occur. Of course the allowable discharge power would scale with thruster size and a review of limiting discharge powers on thrusters having various diameters has suggested that it is probably the discharge power per unit beam area (P_D/A_B) that defines this constraint.

The discharge power can be expressed in terms of the energy cost of a beam ion (ϵ_B) through the equation

$$\frac{P_D}{A_B} = \frac{\epsilon_B J_B}{A_B} \quad . \tag{13}$$

Combining Eqs. 1, 8 and 13 one can obtain

$$P_B = \left[\frac{P_D}{A_B}\right]\left[\frac{A_B}{\epsilon_B}\right]\left[\frac{m_i}{2e}\right]\left[\frac{I_{sp}\, g_{eo}}{\eta_u\, F_c\, \alpha}\right]^2 \quad . \tag{14}$$

The beam ion energy cost appearing in this equation can be computed using Brophy's model[11] in the form

$$\epsilon_B = \frac{\epsilon_p^*}{f_B}\left[1-\exp\left(-B_o(1-\eta_u)\right)\right]^{-1} + \frac{f_c\, V_D}{f_B} \tag{15}$$

where the baseline plasma ion energy cost (ϵ_p^*) can be computed when the propellant and discharge voltage (V_D) are prescribed[11] and the extracted ion fraction (f_B) and the fraction of the ions produced that go to cathode potential surfaces (f_c) can be determined when the magnetic field and electron source location are specified.[5] The parameter B_o is given by

$$B_o = \dot{m}\, C_o = \frac{4\,\sigma_o'\,\ell^*}{m_i\, v_o\, \phi_o}\left[\frac{\dot{m}}{A_B}\right] \tag{16}$$

where the primary electron utilization factor (C_o), the primary electron/propellant atom total inelastic collision cross section[11] (σ_o'), the primary electron containment length (ℓ^*),[11] the propellant atom thermal velocity (v_o) and the transparency of the grids to neutral atoms (ϕ_o) may be assumed constant for a particular propellant and discharge voltage. An expression for the propellant flowrate per unit beam area needed in Eq. 16 can be obtained by combining the definition of propellant utilization efficiency

$$\eta_u = \frac{J_B\, m_i}{\dot{m}\, e} \tag{17}$$

with Eqs. 2 through 7 to obtain

$$\frac{\dot{m}}{A_B} = \frac{2\,\epsilon_o\, \mathbb{F}\, \phi_s\, \psi_e}{9\,\eta_u^4\,\ell_e^2\,R^{3/2}}\left[\frac{m_i}{e}\right]^2\left[\frac{I_{sp}\, g_{eo}}{F_c\,\alpha}\right]^3 \quad . \tag{18}$$

Equations 14, 15, 16 and 18 when combined with an operational objective yield the beam power/beam area/specific impulse surface that defines the discharge power per unit beam area constraint.

Screen Grid Lifetime Constraint

Although the screen grid is assumed to be the life limiting component subjected to sputter erosion in this paper, additional constraints pertaining to other components that are subjected to ion bombardment could impose similar constraints. They would be incorporated into the analysis in the same way as the one developed here for the screen grid. If the screen grid lifetime is considered to have expired when a fraction γ_s of its initial thickness t_s has been sputtered away[8] then this lifetime will be given by

$$r_s = \frac{e \rho N_a \gamma_s t_s}{\left[j_+ S_s^+(V_D) + 0.5\, j_{++} S_s^{++}(2V_D)\right] M} \qquad (19)$$

where ρ and M are the density and molecular weight of the grid material, N_a is Avagadro's number, j_+ and j_{++} are the singly and doubly charged ion current densities striking the grid and $S_+(V_D)$ and $S_{++}(2V_D)$ are the sputtering yields of the grid material for singly and doubly charged ions evaluated respectively for ions with energies equal to the discharge voltage and twice the discharge voltage. Recognizing that the grid will sputter most rapidly at the point of maximum current density ($j_+ = j_{max}$) Eqs. 1, 2 and 8 can be combined with Eq. 19 to obtain

$$P_B = \frac{m_i \rho N_a \gamma_s t_s \mathbb{F} A_B}{2 r_s M \left[S_s^+(V_o) + 0.5 \frac{j_{++}}{j_+} S_s^{++}(2V_o)\right]} \left[\frac{I_{sp} g_{eo}}{\eta_u F_t \alpha}\right]^2 . \qquad (20)$$

The doubly-to-singly charged ion current density ratio (j_+/j_{++}) appearing in this equation is a strong function of discharge operating conditions and is given by[11]

$$\frac{j_{++}}{j_+} = \frac{2\left[Q_o^{++} + \frac{n_p}{n_M} P_o^{++}\right]}{Q_o^+ + \frac{n_p}{n_M} P_o^+} + 0.83 \left(\frac{v_o}{v_b}\right)\left(\frac{\phi_o}{\phi_s}\right)\left[\frac{Q_+^{++} + \frac{n_p}{n_M} P_+^{++}}{Q_o^+ + \frac{n_p}{n_M} P_o^+}\right] \frac{\eta_u}{1-\eta_u} . \qquad (21)$$

Some simplification of this equation is generally possible because the first term is negligible at typical discharge chamber electron temperatures and energies. In Eq. 21 v_b and v_o are the Bohm[12] and neutral atom thermal velocities, ϕ_s and ϕ_o are the transparencies of the grids to ions and neutral atoms and Q_o^+, P_o^+ and etc. are the rate factors associated with production of the various ionic species.[13] The primary-to-Maxwellian electron density ratio (n_p/n_M) appearing in Eq. 21 is given by[11]

$$\frac{n_p}{n_M} = \left\{\left[\frac{0.15\, e\, \epsilon_p^*\, v_b\, \phi_o\, \phi_s}{v_p\, V_D\, f_B\, \sigma_o'}\right]\left(\frac{A_B}{\dot{m}}\right)\left(\frac{A_B}{\Psi}\right)\left(\frac{1}{1-\eta_u}\right)^{-1} - 1\right\}^{-1} \qquad (22)$$

In this equation, the primary electron velocity (v_p) is determined by its energy which is assumed in turn to be equal to the discharge voltage. The discharge chamber volume-to-beam area ratio (Ψ/A_B) is simply the discharge chamber length which may be assumed to be relatively insensitive to beam area (e.g. $\Psi/A_B = 0.1 + 0.1\,[1-\exp(-10A_B)]$ has been used for the examples presented here). The final expression needed to define the screen grid lifetime constraint is one for the propellant mass flowrate per unit beam area. It is obtained by combining Eqs. 1, 8 and 17.

$$\frac{\dot{m}}{A_B} = \frac{2 P_B \eta_u}{A_B} \left[\frac{F_t \alpha}{I_{sp} g_{eo}}\right]^2 \qquad (23)$$

Equations 20 through 23 can be solved for the beam power/beam area/specific impulse surface that defines the screen grid lifetime constraint when an operational constraint is specified and design definitions associated with the chamber (e.g., propellant, discharge voltage, etc.) have been made.

Accel Grid Lifetime Constraint

For a three-grid ion optics system where sputtering on the barrel (interior surface) region of the accel grid holes dominates the erosion of the grid, the change in accel hole diameter (d_a) per unit time is given by

$$\frac{d(d_a)}{dr_a} = \frac{S_a j_{max} n_o \sigma_{ce} \Psi_{ce} f_a M}{e N_a \rho \pi d_a t_a} . \qquad (24)$$

In this equation S_a is the sputter yield of the accelerator grid material at the prevailing charge exchange ion kinetic energy, n_o is the neutral atom density in the charge exchange reaction region, Ψ_{ce} is the volume of this region, f_a is a factor that describes the extent to which these ions are focused or distributed along the barrel region and t_a is the accelerator grid thickness. For a two-grid optics set where sputtering on the downstream surface of the accel grid dominates, a similar equation[6] is used but for the example being considered here, the three-grid equation (Eq. 24) will be used exclusively.

The neutral atom density in the charge exchange region is given approximately by the expression

$$n_o = \frac{4 J_B (1-\eta_u)}{A_B \phi_o v_o e} . \qquad (25)$$

If the allowable change in diameter is Δd_a and τ_a is the desired lifetime then the integrated form of Eq. 24 may be combined with Eqs. 1, 2, 8 and 25 to obtain

$$P_B = \frac{A_B m_i}{4} \left[\frac{\mathbb{F} \phi_o v_o N_a \rho t_a (\Delta d_a/d_a)}{\tau_a S_a (1-\eta_u) \sigma_{ce} f_a M \ell_g}\right]^{1/2} \left[\frac{I_{sp} g_{eo}}{\eta_u F_t \alpha}\right]^2 . \qquad (26)$$

In order to compute beam power as a function of beam area and specific impulse using this equation the volume of the charge exchange region has been assumed to be equal to that of the cylinder shown in Fig. 1 with a diameter equal to that of the accel grid aperture (d_a) and a length twice the grid separation distance (ℓ_g). In addition the ratio of accel grid thickness to grid separation distance (t_a/ℓ_g) has been assumed to be constant.

Operational Objective

It is necessary to define an operational objective for a thruster in addition to the various physical constraints imposed on it in order to define the thruster discharge chamber operating point, i.e., the propellant utilization efficiency and discharge power at which the thruster should be operated. This can be done for example by defining a mission of interest, which might be characterized by a mission time and characteristic velocity or a complex mission algorithm; computing the masses of the system elements (power plant, propellant, payload, etc.) and determining the propellant utilization efficiency operating point at which the associated payload fraction is maximized. The optimum propellant utilization operating point has been selected in this study so the thruster operates at the maximum thrust-to-power condition.[14] This condition is defined by combining Eqs. 1, 5, 6, 7, and 17 with the expression for thruster electrical efficiency which is given by

$$\eta_e = \frac{P_B}{P_T} = \frac{J_B V_B}{J_B V_B + \Sigma P} . \qquad (27)$$

In this equation P_T is the total thruster power and ΣP is the sum of the powers needed to generate ions and to sustain thruster temperatures, propellant flow-rates and neutralizer operation (i.e., the power loss term). Frequently the dominant power loss is the discharge power required to produce the

ions and it can be expressed in terms of the energy cost of a beam ion ($P_D = J_B \epsilon_B$). Assuming the discharge power does dominate the losses, Eq. 27 can be rewritten as

$$\eta_e = \frac{V_B}{V_B + \epsilon_B} \tag{28}$$

and this equation can be combined with those identified above to obtain the expression for thrust-to-total power.[14]

$$\frac{F}{P_T} = \frac{I_{sp}\, g_{eo}}{\eta_u} \left[\frac{1}{\frac{1}{2}\left(\frac{I_{sp}\, g_{eo}}{\eta_u F_t \alpha}\right)^2 + \frac{\epsilon_B e}{m_i}} \right] \tag{29}$$

By seeking the propellant utilization that maximizes this equation at each specific impulse, operation at maximum thrust-to-power is realized for each thruster beam area and physical constraint condition.

RESULTS

The analysis technique outlined in the preceeding section can be used to investigate the effects of a wide variety of design and operational parameters on the power and thrust capabilities of ion thrusters. Because the purpose of this paper is to demonstrate the capability of the methodology involved rather than to draw conclusions based on an exhaustive study conducted using it, one set of typical values of thruster parameters has been selected for use in the analysis. The values used are listed in Table I and while they are considered to be typical of ion thrusters in general, they do not represent any particular thruster. The rate factors used in the analysis are based on an assumed Maxwellian electron temperature of 5 eV and a primary electron energy, which is consistent with the discharge voltage (30 eV).

Table I. Thruster Parameters Used in Example Study in the Order of Their Appearance

Parameter/Property	Symbol	Value Used
Ion Beam Flatness	IF	0.5
Ion Current Density Enhancement Factor	ψ_e	1.0
Screen Grid Transparency to Ions	ϕ_s	0.7
Grid System Transparency to Neutral Atoms	ϕ_o	0.16
Ion Mass (Xenon)	m_i	2.2×10^{-25} kg
Net-to-Total Accelerating Voltage Ratio	R	0.5
Beamlet Divergence Thrust Factor	F_t	1.0
Multiply Charged Ion Thrust Factor	α	1.0
Screen Grid Thickness	t_s	5×10^{-4} m
Grid Separation to Screen Hole Diameter Ratio	ℓ_g/d_s	1.0
Baseline Plasma Ion Energy Cost	ϵ_p^*	50 eV/ion
Extracted Ion Fraction	f_B	0.5
Fraction of Plasma Ions Going to Cathode Potential Surfaces	f_c	0.3

Table I (continued).

Parameter/Property	Symbol	Value Used
Discharge Voltage	V_D	30 V
Total Electron-Atom Inelastic Collision Cross Section[15,16]	σ_o'	7.4×10^{-20} m^2
Primary Electron Containment Length	ℓ^*	3.5 m
Neutral Atom Thermal Velocity	v_o	290 m/sec
Allowable Screen Grid Erosion Fraction	γ_s	0.5
Ionization Rate Factors for 5 eV Temperature Maxwellian Electrons[13]	Q_o^+	7.1×10^{-15} m^3/sec
	Q_+^{++}	5.1×10^{-16} m^3/sec
Ionization Rate Factors for 30 eV Energy Primary Electrons[13]	P_o^+	1.3×10^{-13} m^3/sec
	P_+^{++}	2.5×10^{-14} m^3/sec
Sputter Yields for Molybdenum Screen Grid for Singly and Doubly Charged Ions[17]	S_s^+	2×10^{-6}
	S_s^{++}	1.5×10^{-3}
Sputter Yield for Accel Grid[17]	S_a	1.0
Charge Exchange Cross Section[18]	σ_{ce}	3×10^{-19} m^2
Accel Grid Thickness-to-Grid Separation Ratio	t_a/ℓ_g	0.3
Allowable Accel Grid Erosion	$\Delta d_a/d_a$	0.5
Charge Exchange Ion Focusing Factor	f_a	0.25

If one prescribes a thruster with a beam area of 0.2 m^2 and calculates the beam power limits for each of the physical constraints described in the preceeding section with the objective of operation at maximum thrust-to-power, the curves of Fig. 2 are obtained for the values of the constraints cited in the figure. For each constraint, operation below and to the right of the associated curve assures operation that does not violate the constraint. Hence in the case of Fig. 2 the 600 span-to-gap constraint limits the power that can be extracted up to a specific impulse of ~3000 sec and then the

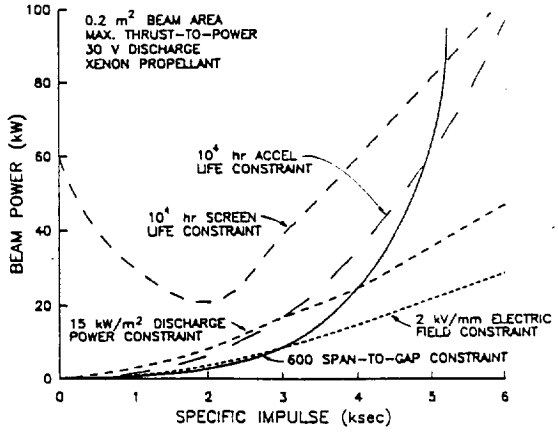

Fig. 2. Typical Power Constraint Curves - 0.2 m^2 Beam Area (Span-to-Gap and Intragrid Electric Field Limiting)

2 kV/mm electric field constraint becomes limiting. For the particular parameters associated with the other constraints, Fig. 2 indicates none of the other constraints (discharge power, screen grid life, or accel grid life) become limiting at any specific impulse up to 6000 sec. The fact that span-to-gap is limiting at low specific impulses while electric field becomes limiting at higher ones is in qualitative agreement with experimental observations.

If the grids were designed so the electric field limit could be increased to 4 kV/mm and the other constraints were held fixed at the values of Fig. 2, then the data of Fig. 3 are generated. They suggest the 600 span-to-gap limit would prevail to ~4000 sec. specific impulse and the discharge power per unit beam area limit of 15 kW/m² would become constraining beyond that point. Increasing the electric field limit has in this case allowed the beam power at 4000 sec I_{sp} to increase from ~15 kW (Fig. 2) to ~25 kW (Fig. 3) and at 6000 sec from ~27 kW (Fig. 2) to ~45 kW (Fig. 3). If, on the other hand, it were necessary to have screen and accel grid lifetimes of 2 x 10^4 hr then the accelerator grid lifetime would become limiting over the I_{sp} range from about 3500 sec to 4500 sec as the data of Fig. 4 show. In this case the power at 4000 sec I_{sp} would be limited by accel grid lifetime considerations to ~21 kW.

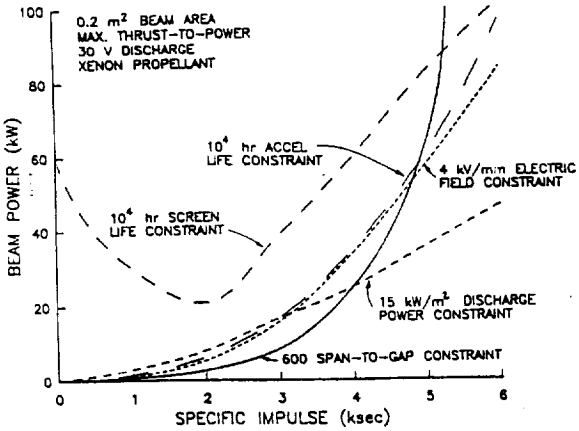

Fig. 3. Typical Power Constraint Curves - 0.2 m² Beam Area (Span-to-Gap and Discharge Power Limiting)

If the beam power limits imposed by the constraints being considered as functions of both beam area and specific impulse are sought rather than holding beam area constant, then beam power/beam area/specific impulse surfaces like those shown in Fig. 5 are generated. These surfaces define power limits associated with each constraint indicated and they are all plotted on the same scale, namely the one defined in Fig. 5a. Operation is permitted at any point beneath the surface associated with a particular constraint, but not above it. All of these surfaces behave as one would expect with the beam powers being lowest for low beam areas and low specific impulses except the one associated with screen grid lifetime. The high allowable power observed at low specific impulses for the screen life constraint seems unusual. It is a consequence of operation at maximum thrust-to-power which implies a low propellant utilization at low specific impulses (Eq. 29). Low propellant utilizations in turn imply low doubly-to-singly charged ion current densities (Eq. 21) and hence high allowable beam powers (Eq. 20).

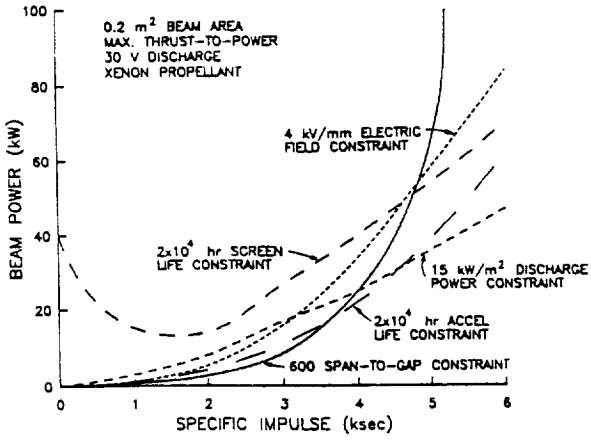

Fig. 4. Typical Power Constraint Curves - 0.2 m² Beam Area (Span-to-Gap, Discharge Power and Accel Grid Lifetime Limiting)

When all constraints shown in Fig. 5 are applied and the overall limiting surface is identified, the one shown in Fig. 6 is obtained. As the labels on this surface indicate, the span-to-gap and electric field constraints represent the most restrictive limitations (span-to-gap at low specific impulses and electric field at higher ones) over the beam area range from zero to 1 m².

If one defines a mission along with powerplant and power processor specific mass parameters and then imposes the power limits defined by all of the constraints associated with the data in Fig. 5, payload fractions can be computed as a function of beam area and specific impulse. Figure 7 shows the payload fraction surface computed when the most restrictive of these constraints are applied for a 10^4 m/sec mission to be accomplished in 0.67 year when the powerplant and power conditioner are characterized by the specific masses and the power conditioner efficiency values cited on the figure. The payload fraction reaches a relatively flat peak at a value of 55 percent when the specific impulse is near 4500 sec for all but the smallest beam areas. The payload fraction peak in Fig. 7 is seen to be very broad, so the thruster could be operated at specific impulses ranging from ~3000 to 6000 sec and deliver about the same payload fraction.

The thrust at which the ion thruster operates can also be computed as a function of beam area and specific impulse by using Eqs. 28 and 29 in conjunction with the most restrictive beam power constraining surface data (Fig. 6). Figure 8 shows how the thrust associated with the constraints defined in Fig. 5 would vary as a function of beam area and specific impulse.

If the electric field constraint is increased to 4 kV/mm, the results of Fig. 3 showed that the discharge power per unit beam area became the power-limiting surface at high specific impulses when the beam area was 0.2 m². The effect of introducing this new electric field constraint for beam areas ranging from zero to 1.0 m² is shown in Fig. 9. Comparison of the data in Figs. 6 and 9 shows that increasing the electric field limit facilitates a substantial increase in beam power at high beam area and specific impulse values (250 kw vs. 150 kw).

If the grid lifetime constraints are tightened by requiring 20,000 hr operating times, then the accel grid lifetime constraint identified in Fig. 10 limits the beam power in the moderate specific impulse-low beam area regime. Away from this region

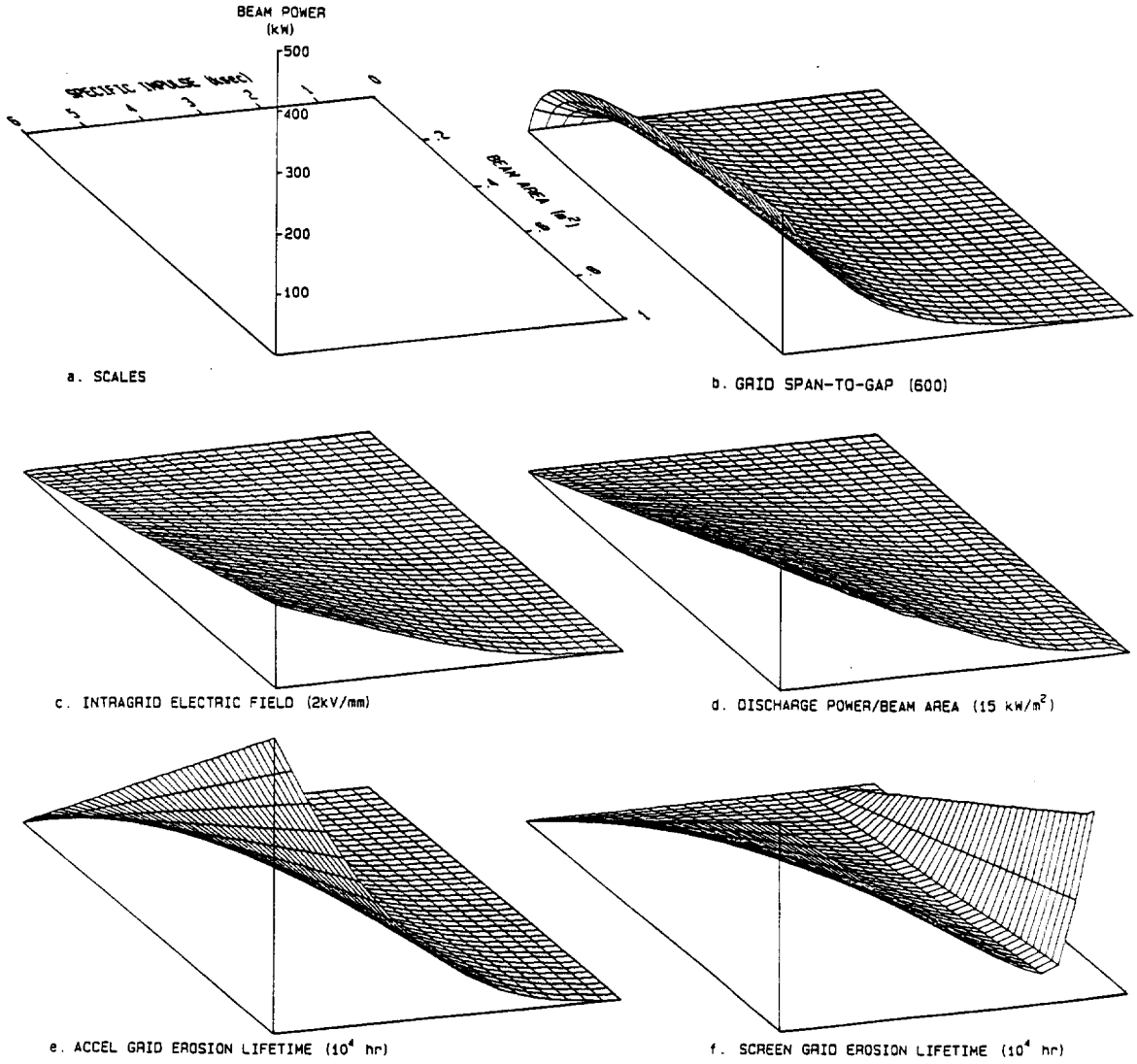

Fig. 5. Typical Power Constraining Surfaces

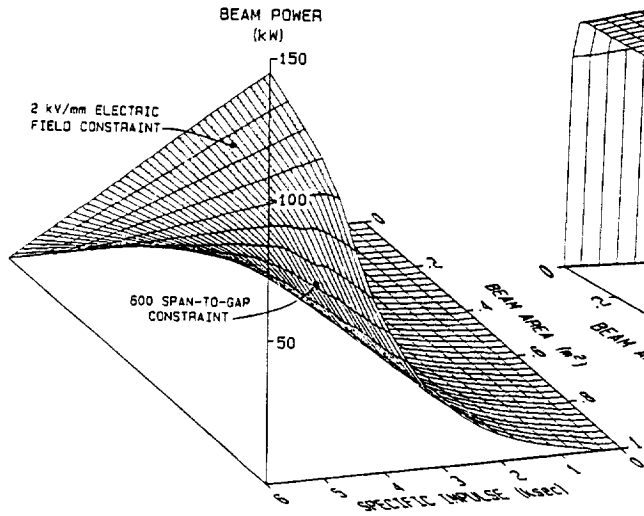

Fig. 6. Typical Overall Power Constraining Surface (Span-to-Gap and Intragrid Electric Field Limiting)

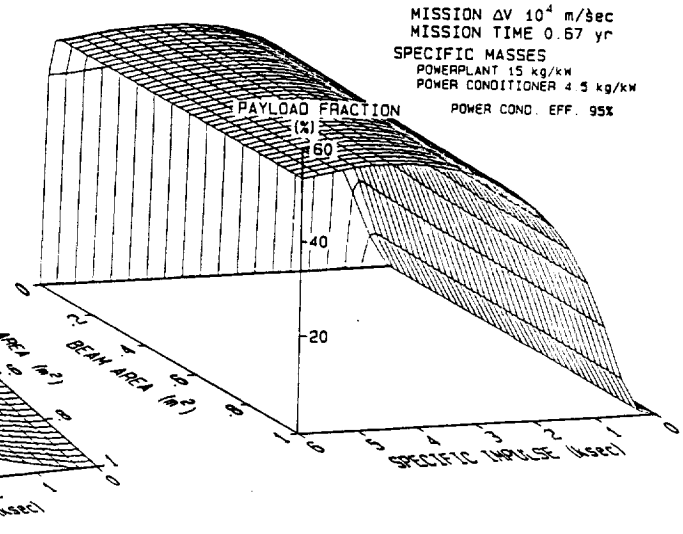

Fig. 7. Typical Payload Fraction Surface

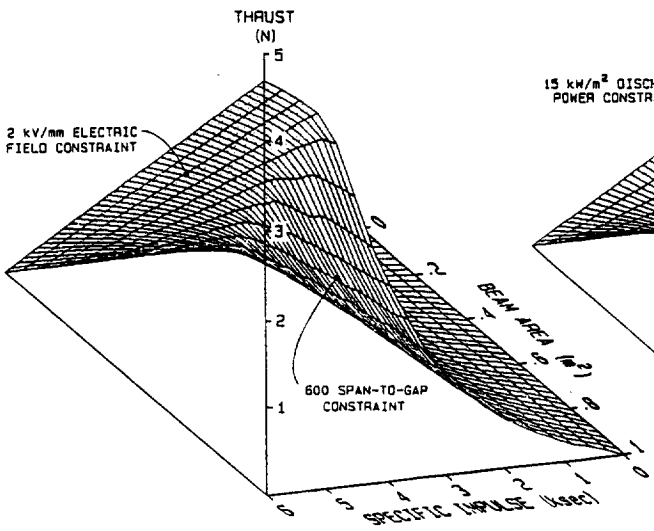

Fig. 8. Typical Thrust Surface

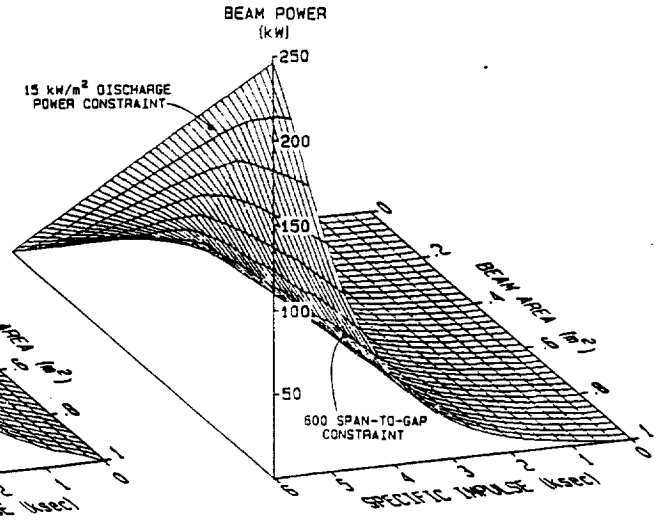

Fig. 9. Typical Overall Power Constraining Surface (Span-to-Gap and Discharge Power Limiting)

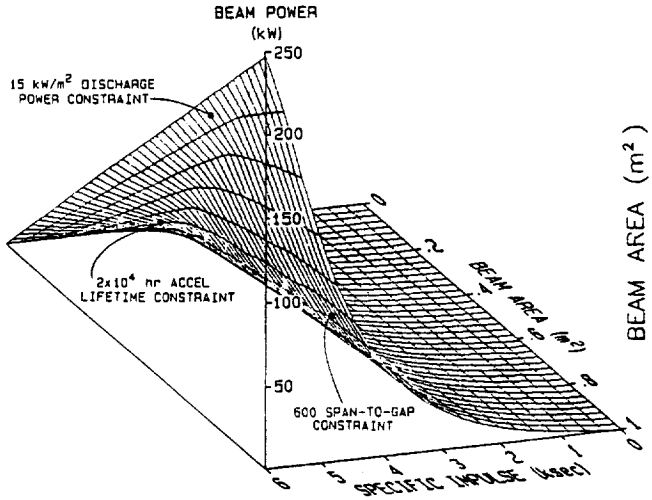

Fig. 10. Typical Overall Power Constraining Surface (Span-to-Gap, Discharge Power and Accel Grid Life Limiting)

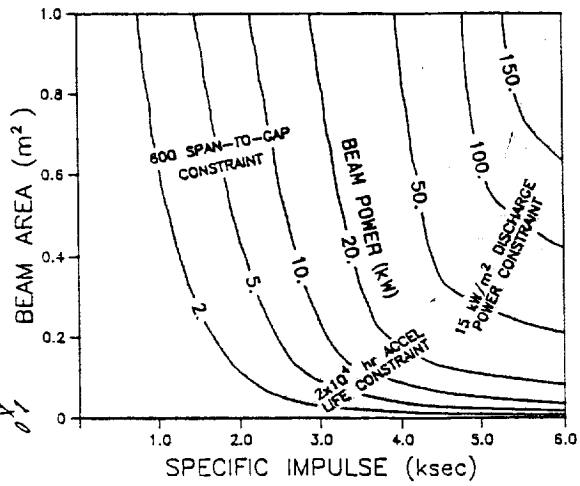

Fig. 11. Constant Power Contour Diagram (Span-to-Gap, Discharge Power and Accel Grid Life Limiting)

the power limit is unchanged from the values presented in Fig. 9.

The three-dimensional plots shown in Figs. 5 through 10 are useful to illustrate qualitative behavior, but they are difficult to use as a source of quantitative information. Quantitative information can be presented better in the form of an equal beam power contour plot like the one in Fig. 11. This figure, which presents the same data as that in Fig. 10, clearly indicates the beam power limit at any beam area and specific impulse point. It also shows the constraint that is preventing operation at higher power levels at each beam area and specific impulse. Similar figures could, of course, also be generated to show the limiting values of thrust and payload fraction as a function of thruster beam area and specific impulse.

FUTURE DIRECTIONS

The intent of the preceding discussion has been 1) to present a methodology and framework within which gross parameters describing ion thruster behavior could be used to predict ion thruster performance limits, 2) to cite references that describe how these gross parameters can be computed, and 3) to suggest how results obtained from the analysis might be presented in a readily understood format. The analysis should, however, not be considered fully developed. The following statements describe changes that might be introduced to improve the analysis.

1) The beamlet divergence (thrust) factor (F_t), the grid separation-to-screen hole diameter ratio (ℓ_g/d_s) and the net-to-total acceleration voltage ratio (R) have all been treated as constants in the cases presented. These quantities are, however, variable and they are related to each other. One could therefore use data like those in Ref. 19 to determine values of F_t for prescribed values of ℓ_g/d_s and R or one could incorporate additional operational objectives that would assure the parameters are selected to maximize a thruster parameter of interest.

2) The screen and accel grid thicknesses (t_s and t_a respectively) have been treated as constants, and depending on the beam geometrical cross section

it may be that they would be better represented as functions of beam area. For example, a functional relationship between these thicknesses and the beam area based on mechanical deformation considerations might be desirable.

3) Although some variation in discharge chamber plasma properties has been allowed in the development of the screen life constraint, more can be done in modeling the other constraints to reflect the effects of changes in Maxwellian electron temperature, primary and Maxwellian electron densities, the baseline plasma ion energy cost (ϵ_p^*) and the doubly-charged ion thrust factor (α) induced by changes in propellant utilization and discharge voltage. It is noted that the physically based models needed to do this are available.[20]

4) The grid spacing has been assumed constant across the entire intragrid region. The effects of variable spacing induced by grid thermal distortion and electric field induced deflection forces may cause this spacing to change as a function of location on the grids. This in turn will influence the ion extraction and electrical breakdown capabilities of the grids.

Finally, it is noted that many of the parameters needed to model the plasma discharge and ion extraction phenomena involved in this analysis can be computed from basic principles. The noteworthy exception to this is the primary electron containment factor ℓ^*. It can be inferred from discharge chamber tests,[11] but a model that can be used to calculate it for a discharge chamber having prescribed dimensions and magnetic field characteristics is needed. Additional work may also be needed to describe more accurately the energy of primary electrons extracted from a hollow cathode as a function of discharge voltage.

CONCLUSIONS

A methodology that can be used to determine the maximum power level at which an ion thruster can be operated and a framework within which the resultant data can be presented has been developed. Physical constraints associated with the allowable grid span-to-gap ratio, the intragrid electric field, the discharge power per unit beam area and the screen and accel grid lifetimes have been identified as power (or thrust) limiting and relationships that quantify each of the constraints have been presented. When the methodology is exercised for a thruster operating on xenon at propellant utilization efficiencies that induce maximum thrust-to-power with constraints of 600 span-to-gap ratio, 2 kV/mm electric field, 15 kW/m^2 discharge power per unit beam area and 10^4 hr screen and accel grid lifetime requirements, the span-to-gap constraint is shown to be limiting at low specific impulses and the electric field is shown to be limiting at higher ones. If the electric field limit is increased to 4 kV/mm, the discharge power becomes limiting at high specific impulses and if the grid lifetime requirement is increased to 2 x 10^4 hr then accel grid erosion can become limiting at intermediate specific impulses. Although the input data have not been selected so results predicted in the analysis can be compared to experimental observations, the general trends appear to be consistent with generally observed experimental trends.

REFERENCES

1. Byers, D. C. and V. K. Rawlin, "Critical Elements of Electron-Bombardment Propulsion for Large Space Systems," Jour. of Spacecraft and Rockets, V. 14, Nov. 1977, pp. 648-654.

2. Byers, D. C., "Characteristics of Primary Electric Propulsion System," AIAA Paper 79-2041, Oct. 31-Nov. 2, 1979.

3. Kaufman, H. R., "Technology of Electron-Bombardment Ion Thrusters," Advances in Electronics and Electron Physics, V. 36, Ed. L. Marton, Academic Press, New York, 1974, pp. 265-373.

4. Rovang, D. C., "Ion Extraction Capabilities of Two-Grid Accelerator Systems," NASA Contactor Report CR-174621, Feb. 1984.

5. Arakawa, Y. and P. J. Wilbur, "Discharge Plasma Calculations in Cusped Ion Thrusters Using the Finite Element Method," Paper 88-079, 20th AIAA/DGLR/JSAS International Electric Propulsion Conference, Oct. 3-6, 1988, Garmisch-Partenkirchen, W. Germany.

6. Langmuir, I., "The Interaction of Electron and Positive Ion Space Charges in Cathode Sheaths," Phys. Rev., V. 33, 1929, p. 954.

7. Feng, Y. and P. J. Wilbur, "Enhancement of Ion Beam Currents through Space-Charge Compensation," J. Appl. Phys., V. 54, No. 11, Nov. 1983, pp. 6113-6118.

8. Poeschel, R. L. and J. R. Beattie, "Primary Electric Propulsion Technology Study," Final Report on Contract NAS 3-21040, pp. 127-154.

9. Kaufman, H. R., "Accelerator-System Solutions for Broad-Beam Ion Sources," AIAA Jour., V. 15, July 1977, pp. 1025-1034.

10. Aston, G. and P. J. Wilbur, "Ion Extraction from a Plasma," J. Appl. Phys., V. 52, April 1981, pp. 2614-2626.

11. Brophy, J. R., "Ion Thruster Performance Model," NASA CR-174810, Dec. 1984.

12. Bohm, D., "Minimum Ionic Kinetic Energy for a Stable Sheath," in Characteristics of Electrical Discharges in Magnetic Fields, A. Guthrie and R. K. Wakerling, eds., McGraw-Hill, Inc., New York.

13. Wilbur, P. J. and H. R. Kaufman, "Double Ion Production in Argon and Xenon Ion Thrusters," Jour. of Spacecraft and Rockets, V. 16, July-Aug. 1979, pp. 264-267.

14. Beattie, J. R. et al., "Xenon Ion Propulsion Subsystem," AIAA Paper 85-2012, Sept.-Oct. 1985.

15. Hayashi, M., "Determination of Electron-Xenon Total Excitation Cross Sections, from Threshold to 100 eV, from Experimental Values of Townsend's α," Journal of Physics D: Applied Physics, V. 16, 1983, pp. 581-589.

16. Rapp, D. and P. Englander-Golden, "Total Cross Sections for Ionization and Attachment in Gases by Electron Impact. I. Positive Ionization," Journal of Chemical Physics, V. 34, No. 5, 1965, pp. 1464-1479.

17. Bahdansky, J., J. Roth and H. L. Bay, "An Analytical Formula and Important Parameters for Low-Energy Ion Sputtering," J. Appl. Phys., V. 51, May 1980, pp. 2861-2865.

18. Rapp, D. and W. E. Francis, "Charge Exchange between Gaseous Ions and Atoms," J. of Chem. Phys., V. 37, Dec. 1962, pp. 2631-2645.

19. Aston, G. and H. R. Kaufman, "Ion Beam Divergence Characteristics of Three-Grid Accelerator Systems," AIAA Jour., V. 17, No. 1, Jan. 1979, pp. 64-70.

20. Brophy, J. R. and P. J. Wilbur, "Calculation of Plasma Properties in Ion Sources," AIAA Jour., V. 24, No. 9, Sept. 1986, pp. 1516-1523.